Petroleum Science 20 (2023) 577–589

Contents lists available at ScienceDirect

Petroleum Science

journal homepage: www.keaipublishing.com/en/journals/petroleum-science

Original Paper

Temperature/salt tolerance and oil recovery of xanthan gum solution enhanced by surface-modified nanosilicas

Long Xu [a, b, *], Xu Liu [a], Hong-Yu Ding [a], Huan Zhang [a], Lei Liu [c], Jing-Hui Li [c], Hou-Jian Gong [a, b], Ming-Zhe Dong [a, b]

[a] Shandong Key Laboratory of Oilfield Chemistry, School of Petroleum Engineering, China University of Petroleum (East China), Qingdao, Shandong, 266580, China
[b] Key Laboratory of Unconventional Oil & Gas Development (China University of Petroleum (East China)), Ministry of Education, Qingdao, Shandong, 266580, China
[c] Northwest Company of China Petroleum and Chemical Corporation, SINOPEC, Urumqi, Xinjiang, 830011, China

ARTICLE INFO

Article history:
Received 6 May 2022
Received in revised form
16 June 2022
Accepted 16 August 2022
Available online 20 August 2022

Edited by Jia-Jia Fei

Keywords:
Temperature/salt tolerance
Rheology
Surface-modified nanosilicas
Xanthan gum
Enhanced oil recovery
Synergy

ABSTRACT

Amide- and alkyl-modified nanosilicas (AANPs) were synthesized and introduced into Xanthan gum (XG) solution, aiming to improve the temperature/salt tolerance and oil recovery. The rheological behaviors of XG/AANP hybrid dispersions were systematically studied at different concentrations, temperatures and inorganic salts. At high temperature (75 °C) and high salinity (10,000 mg·L^{-1} NaCl), AANPs increase the apparent viscosity and dynamic modulus of the XG solution, and XG/AANP hybrid dispersion exhibits elastic-dominant properties. The most effective concentrations of XG and AANP interacting with each other are 1750 mg·L^{-1} and 0.74 wt%, respectively. The temperature tolerance of XG solution is not satisfactory, and high temperature further weakens the salt tolerance of XG. However, the AANPs significantly enhance the viscoelasticity the XG solution through hydrogen bonds and hydrophobic effect. Under reservoir conditions, XG/AANP hybrid recovers approximately 18.5% more OOIP (original oil in place) than AANP and 11.3% more OOIP than XG. The enhanced oil recovery mechanism of the XG/AANP hybrid is mainly increasing the sweep coefficient, the contribution from the reduction of oil-water interfacial tension is less.

1. Introduction

Recently, biopolymer nanocomposites have been of significant interest in industrial applications due to controlled electric, optic, and mechanic properties (Balazs et al., 2006), and composites are widely used in coatings, wastewater treatment, oil recovery and so on (Shoichet, 2010; Gregory and Barany, 2011; Xu et al., 2021). Due to the small size effect and stable performance in harsh environments (Batista et al., 2015), the introduction of nanoparticles (NPs) into biopolymers to prepare nanocomposites improves the strength of biopolymers (Yi et al., 2020). Meanwhile, the biopolymers also bring advantages to nanocomposites related to their biocompatibility and biodegradability. Among the biopolymers, microbial exopolysaccharides exhibit interesting features in stabilizing, emulsifying, thickening and gelation (Paul et al., 1986; Maruyama et al., 2007; Moreira et al., 2011) and are expected to be alternatives to products in the chemical industry.

The interaction between polymer molecules and particles has been intensively studied. In general, the steric stabilization of particulate gels is affected by the interaction between macromolecules-macromolecules, particles-particles, and macromolecules-particles. The molecular conformation of polymers adsorbed at the particle interfaces depends on their charges and ionic strength. Particle loadings on the polymer molecules are determined by the number of groups contributing to hydrogen bonds (Kennedy et al., 2015). Depending on the interaction between the polymer molecular chains and the particle surface, the molecular conformation of aggregates and the influence on material properties vary drastically for particles on the nanoscale (Srivastava et al., 2014). The NPs not only increase the viscosity of the polymer with similar size, but also enhances the

* Corresponding author. Shandong Key Laboratory of Oilfield Chemistry, School of Petroleum Engineering, China University of Petroleum (East China), Qingdao, Shandong, 266580, China.
E-mail address: xulong@upc.edu.cn (L. Xu).

https://doi.org/10.1016/j.petsci.2022.08.020

mechanical performance of the polymer molecular conformation (Cheng et al., 2017; Wang et al., 2022). Hu et al. (2017) have reported that nanosilica enhances the viscosity of a hydrophobically associating polyacrylamide (HAPAM) solution due to hydrogen bonds between the SiOH of nanosilica and the amide group of HAHPAM. Xu et al. (2021) found that hydrophobic effects could further improve the rheological behaviors of HPAM/nanosilica composites at high salinity.

It was reported that silicas can promote nongelling polysaccharides, such as hyaluronate and chitosan, gelation (Shchipunov et al., 2005). In the gelation, Oliveira et al. (2010) thought that the nanosilicas around the polysaccharide molecular chains restrained the movement of the molecules and the polysaccharide molecular played a role as a template and chain-connected particles, resulting in the formation of network structures. The gelation phenomenon is more likely to occur in hydrophilic nanosilica and polymers with carbonyl and hydroxyls groups (Persello et al., 2004; Petit et al., 2007). Shchipunov et al. (2005a, b) observed a similar self-assembly behavior in the formation of hydrogels by cationic hydroxyethylcellulose or sodium hyaluronate and silica. However, a network of silica particles generally does not exist spanning the whole dispersion system, and the continuous network is supported by polymer molecular chains (Zhou et al., 2020). In contrast, some researchers reported that the silicas decrease the stability of polysaccharide gels, such as gelatin and carrageenan, by weakening the molecule aggregation (Coradin et al., 2004; Daniel-da-Silva et al., 2008).

Xanthan gum (XG), an extracellular polysaccharide, is already exploited in the pharmaceutical, food, cosmetic and oil recovery industries as a thickener (Gilbert et al., 2013; Xu et al., 2014; Habibpour and Clark, 2017). It is secreted by the bacterium Xanthomonas. The molecular backbone of XG is made up of pentasaccharide repeating units. Trisaccharide side chains consisting of β-D-rhamnopyranosyl, β-1,4-D-glucuronopyranosyl and α-1,2-D-mannopyranosyl are substituted on β-1,4-D-glucopyranosyl in the backbone (De Jong and Van de Velde, 2007). Different content of carboxylic, acetyl and pyruvate groups are located in the side chains. Previous research has demonstrated that XG molecules tend to be a semiflexible state and form single- or double-stranded helices in the solution (Koenderink et al., 2004). XG can inhibit the agglomeration of NPs, such as gold, iron and palladium, by adsorbing to create steric repulsion among the particles (Xue and Sethi, 2012; Pooja et al., 2014). The strongly subdiffusive motion of the NPs in XG solution with a high storage modulus results in the low fractal dimension of the aggregation (Pashkovski et al., 2003). Senanayake and Mukhopadhyay (2019) explained the particle mobility change by hydrodynamic interaction between XG and gold NPs in the semidilute regime. The presence of XG also enhanced the adsorption of hydrophilic NPs at the oil-water interface and effectively improved the stability of the emulsion (Pi et al., 2016). In summary, for previous studies, most researchers put the attention on the interaction between hydrophilic nanosilicas and bipolymers with hydroxyl groups, and the polymers adsorbed on the surface of hydrophilic silicas mainly through hydrogen bonds (Persello et al., 2004; Wang and Somasundaran, 2007). The interaction between XG and surface-modified NPs has not yet been determined, especially under oil reservoir conditions, such as high temperature and high salinity. Consequently, understanding how XG and surface-modified NP interactions influence material properties is necessary for the application of biopolymers for enhanced oil recovery (EOR).

In this work, the NPs were firstly surface-modified with amide and alkyl groups and then introduced into XG solution to form hybrid. The rheological behaviors of the XG/AANP hybrid were systematically investigated in relation to component concentration, temperature and inorganic salts. The objective is to improve the rheology and oil recovery of the XG dispersons at high temperature and high salinity by the combination with AANPs. The study provides a feasible and effective surface modification method for NPs which interact strongly with XG molecules. It may also provide an in-depth understanding of the influence of NPs loading and heating/ionic effects on the rheological behavior and molecular structure of XG, with practical relevance for EOR.

2. Experimental

2.1. Materials

γ-Methacryloxypropyl trimethoxysilane (KH570, 99%), acrylamide (AM, 99.0%), sodium bisulfite ($NaHSO_3$, 99%), potassium persulfate ($K_2S_2O_8$, 99.5%), oxalic acid ($H_2C_2O_4$, 98%), ethanol (EtOH, 99.0%), sodium chloride (NaCl, 99.0%), magnesium chloride ($MgCl_2$, 99.0%), calcium chloride ($CaCl_2$, 96.0%), and fumed silica NP powder (20 nm) were produced by Aladdin Biochemical Technology Co., Ltd., China. The specific surface area of the NP powder was 150 $nm^2 \cdot g^{-1}$. Xanthan gum (XG) was obtained from the Inner Mongolia Fufeng Biotechnology Co., Ltd., China. The average W_m was approximately 2.0×10^6 $g \cdot mol^{-1}$. The chemical structure of the XG molecule is represented in Fig. 1. The viscosity of crude oil without water and gas was 23.4 mPa·s at 75 °C and the density was 0.93 g/cm^3.

2.2. Synthesis of the AANPs

The synthesis of AANPs was performed as follows. First, bare SiO_2 powder was mixed with ethanol solution under continuous stirring, followed by ultrasonication for 5 min, to achieve evenly dispersed. Then, a fixed mass of KH570 and acetic acid was added to the SiO_2 dispersion with continuous stirring for 2 h at 70 °C. A γ-methacryloxypropyl-modified nanoparticle (MNP) dispersion was obtained. Next, a certain concentration of AM solution was prepared, and a small amount of $NaHSO_3$ was added as a reducing agent to inhibit the AM polymerization reaction. After full stirring, the AM solution was dropped into the MNP dispersion at a uniform speed, and then a small amount of $K_2S_2O_8$ was added as an oxidant. Nitrogen was injected into the reaction flask for 30 min, the reaction was stirred for 5 h at 75 °C, and amide- and alkyl-modified nanoparticles (AANPs) dispersion was obtained. Finally, The AANPs dispersion was centrifuged, washed and vacuum dried in sequence to obtain AANP solid powder. The reaction mechanism and synthesis steps of AANP were shown in Fig. 2.

2.3. Characterization of the AANPs

The Fourier transform infrared (FTIR) spectra of AANPs was performed on a Tensor-27 spectrometer (Bruker, Switzerland) with the scanning range of 4000–400 cm^{-1}. The morphology of AANP was captured by a transmission electron microscopy (TEM, JEM-2100UHR, Japan). The thermal stability and composition of the AANPs were investigated on a thermogravimetric (TG) analyzer (Netzsch, Germany). The temperature range is 30–800 °C, and the temperature rise rate was controlled at 10 °C/min. TG and differential thermogravimetric (DTG) data were obtained in the tests.

2.4. Preparation of XG/AANP hybrid

A certain amount of AANP powders were dispersed in distilled water to form a homogeneous dispersion by ultrasonication for 5 min. Then, XG at different concentrations were introduced into the AANP dispersion. The XG and AANPs mixtures were slowly

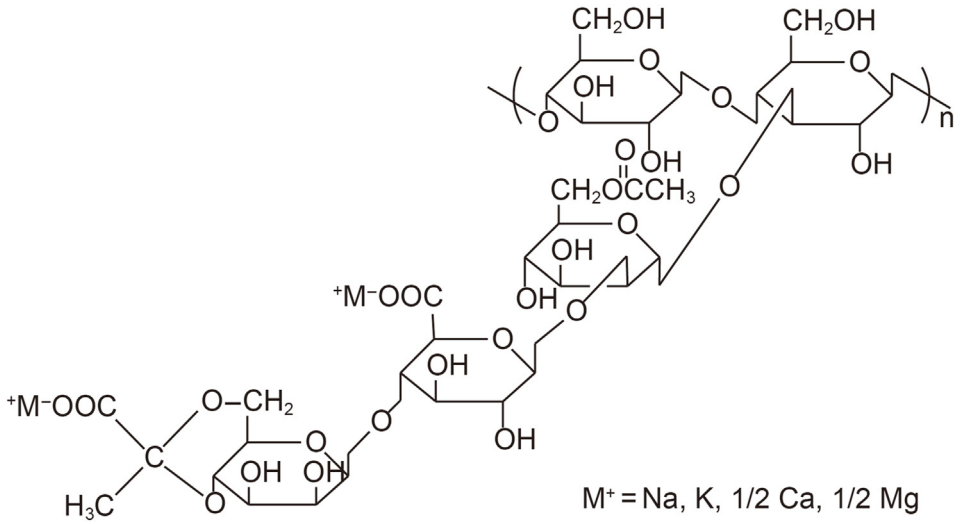

Fig. 1. Molecular structure of XG.

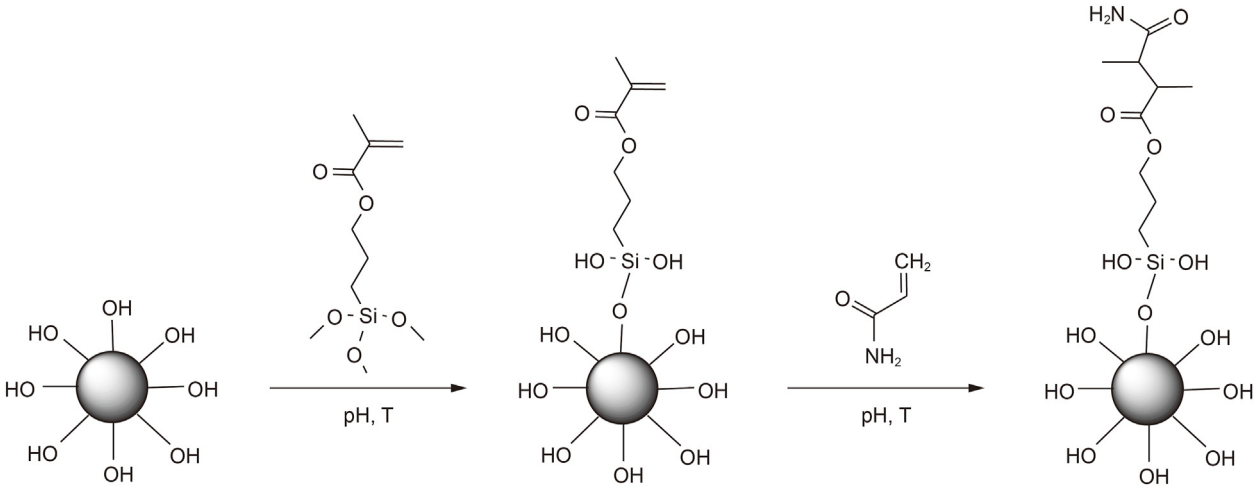

Fig. 2. The synthesis route of AANPs.

stirred for 12 h to give ample time for their contact and interaction. NaCl, $CaCl_2$ and $MgCl_2$ were respectively added to the hybrid dispersion at a certain concentration, followed by stirring for 5 h.

2.5. Rheological measurements

A rotational rheometer (Haake, MARS III, Germany) with concentric cylinder module was used to measure the rheological properties of different systems under steady and oscillatory shear conditions. The steady shear was conducted under a rate-controlled mode, and the apparent viscosity at different shear rates was obtained. Before oscillatory shear, stress-sweep test was carried out to found out the linear viscoelastic region, and dynamic oscillation at different frequencies was conducted in the linear viscoelastic regimes.

2.6. Hydrodynamic length and zeta potential measurements

The hydrodynamic lengths (L) of the sample were determined on a Nano ZS90 Zetasizer (Malvern, UK). The measurement principles are spherical equivalent and dynamic light scattering (DLS) (Edward, 1970). The zeta potentials (ξ) of the sample were determined on the same instrument by measuring the rate of particle movement. The voltage of electric field is 150 V.

2.7. Interfacial tension measurements

Interfacial tension measurements were performed on a TX-500D spinning drop ultra-low interfacial tensiometer at 75 °C. The rotation speed was 5000 r/min, and the measurement time was 1.0 h. All systems reach equilibrium interfacial tension.

2.8. Sandpack flooding tests

The sandpack was evacuated and saturated with formation water, and the pore volume and porosity were measured. The pressure difference between the two ends of the sandpack was measured at different injection rates, and the permeability was calculated by Darcy equation. The permeability of the sandpack used is controlled between 1.0 and 2.0 μm^2, and the porosity is about 40%. The experiments were carried out in a high temperature and high pressure displacement device at 75 °C.

The sandpacking pipe was saturated with crude oil and aged for 3 d. Waterflooding was conducted until the water content of the produced fluid exceeds 98%, and then a 1.0 pore volume (PV) chemical flooding was carried out until the oil content of the produced fluid is less than 2%, and finally the subsequent waterflooding was continued until the oil content in the produced fluid is negligible, and the oil recovery efficiency is calculated. The injection rate was 0.5 mL/min.

3. Results and discussion

3.1. Characteristics of the AANP

The structures of NP and prepared AANP were confirmed with the help of FTIR spectra as shown in Fig. 3. Compared to the NP spectrum, new peaks appear in the AANP spectrum at approximately 2920, 2851 and 1470 cm^{-1} which are attributed to the C–H stretching vibration of $-CH_3$, the C–H stretching vibration of $-CH_2-$ and the C–H in-plane bending vibration, respectively. The peak of AANP at 1632 cm^{-1} is more pronounced, which is attributed to the superposition of the C=O stretching vibration and N–H bending vibration. This confirmed that the amide groups and alkyl chains were grafted onto the nanosilicas.

The micromorphology of the NPs and AANPs observed by TEM are shown in Fig. 4. The agglomeration always occurs in NPs dispersion due to the mutual attraction between particles. For AANPs, the agglomeration of particles weakened and the dispersion performance was improved. It was believed that the amide groups and long alkyl chains increase the steric hindrance between nanosilicas, reducing the contact probability. Meanwhile, the hydrophobicity of the AANPs was enhanced in the presence of alkyl chains, decreasing the attraction between the particles and water molecules. Therefore, the AANPs are well dispersed in aqueous solution.

Fig. 5 shows the TG and DTG results of NP and AANP. It can be seen from the TG curves that when rising the temperature from 30 °C to 140 °C, NP loses 4.0% of the weight, accounting for 50% of the total weight loss, and AANP loses 2% of the weight, accounting for 14% of the total weight loss. The weight loss in this temperature range is the evaporation of adsorbed water on the surface of the nanosilicas and the dehydration-condensation of silanol groups. The surface of nanosilicas has many silanol groups, which are easily pyrolyzed during the heating process (30–140 °C). For AANP, because parts of the silanol groups are replaced, the number of surface silanol groups decreases, and the reduced quality also decreases. During the heating process at 300–500 °C, the quality of AANPs dropped significantly due to the pyrolysis of the acrylamide segments on the surface of the nanosilicas. The result also indicates that many silanol groups are replaced by the acrylamide segments. The DTG curves show one peak at 60 °C for NP and two peaks at 69 °C and 394 °C, respectively, for AANP. The pyrolysis temperature of acrylamide segments is significantly higher than that of hydroxyl groups. The results indicate that acrylamide segments have been grafted on the nanosilicas and have superior thermal stability.

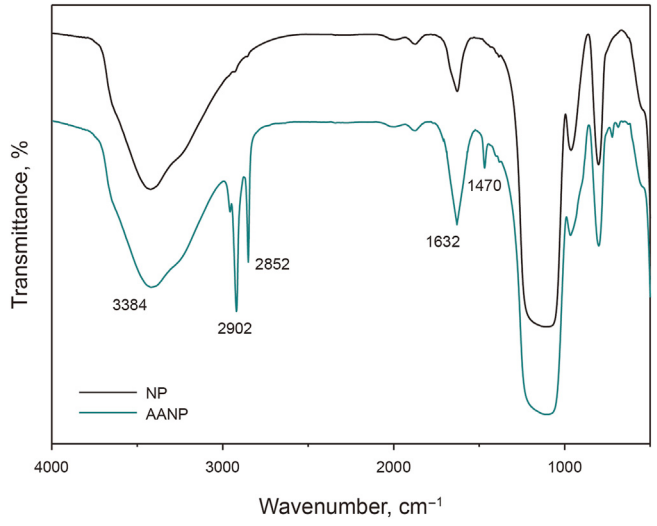

Fig. 3. Infrared spectra of NP and AANP.

3.2. Effect of temperature and salinity on the rheology of XG solutions

A pure aqueous 1750 mg·L^{-1} XG solution exhibits shear thinning behavior when the shear rate exceeds 0.04 s^{-1}, as shown in Fig. 6(a). The marked non-Newtonian behavior of XG solution comes from the changes on molecular aggregate structure. In pure water at a moderate concentration regime, the XG molecular chains were considered semirigid rods with weak self-association through hydrogen bonds (Mao, 2008). At low shear rates, the 1750 mg·L^{-1} XG solution shows a Newtonian plateau. “Domains” of associated XG molecules are not fully occupied in the whole system and broken down under high shears.

The apparent viscosity (η) of XG solution is sensitive to the temperature that η decreases as the temperature increases, as shown in Fig. 6(a). The viscosity retention rate (φ) is defined as the ratio of the apparent viscosity ($\eta_{0.1}$) under different conditions and that at 25 °C in pure water. The φ values of XG at 55 °C and 75 °C are 38.0% and 14.4%, respectively. For the effect of salinity (Fig. 6(b)), η of the XG solution decreases with the addition of NaCl, and the φ value is 60.7%. When the salinity increases from 5000 mg·L^{-1} to 10,000 mg·L^{-1}, η slightly changes.

The rheological behavior of the XG solution can be modeled by the following equations (Mu et al., 2002):

Power-law mode:

$$\eta = k \cdot \dot{\gamma}^{n-1} \tag{1}$$

Cross-empirical mode:

$$\eta = \eta_\infty + \frac{\eta_0 - \eta_\infty}{1 + (\dot{\gamma}/\dot{\gamma}_b)^m} \tag{2}$$

where n is the flow behavior index, k is the consistency index, η_0 *is* the zero-shear viscosity, η_∞ is the infinite-shear viscosity, $\dot{\gamma}_b$ is the critical shear rate, indicating the stability of the molecular structure when the applied stress is applied, and m is the shear rate factor. The rheological parameters fitted by two equations are listed in Table 1. The values of η_0 and η_∞ simultaneously decrease as the temperature increases. All values of n are less than 1 and increase with increasing the temperature, while the k and temperature exhibit opposite changes. When NaCl was added, η_0 and η_∞ of the XG solution decreased, and the variation trend of the rheological parameters was nearly the same for the experimental salinities.

Generally, the viscoelastic properties of fluids are always described by the Maxwell model in which storage modulus (G') and loss modulus (G'') reflect the elastic and viscous components of the fluids, respectively (Xin et al., 2008). The frequency dependence of G' and G'' is expressed in the following equations:

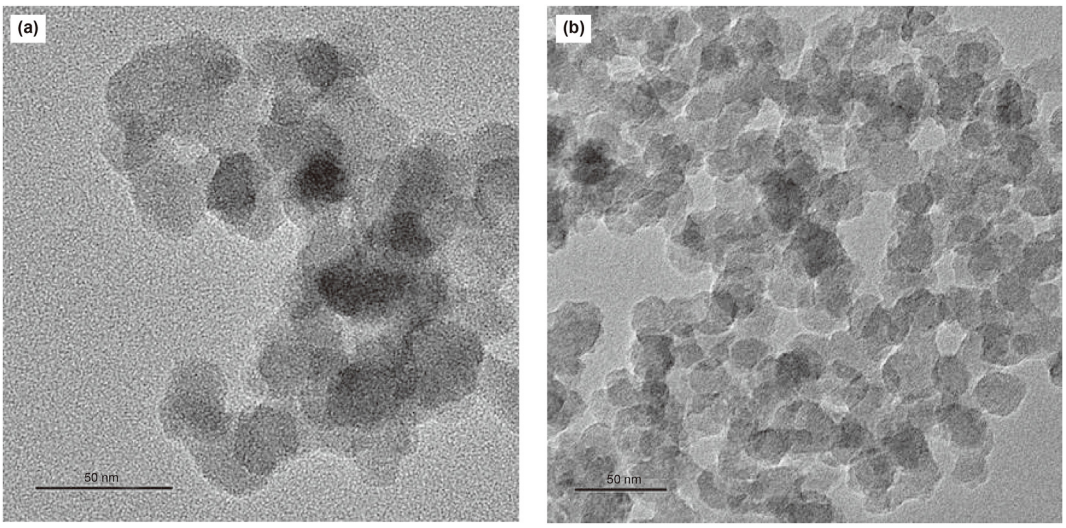

Fig. 4. TEM micrographs of (**a**) NP and (**b**) AANP at 0.1 wt%.

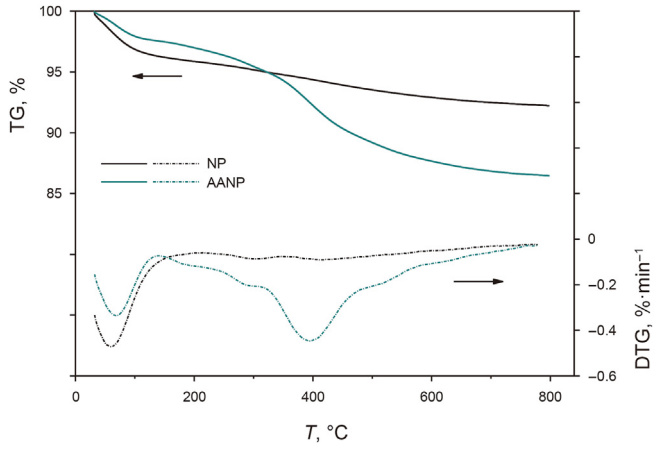

Fig. 5. TG and DTG curves of NP and AANP.

Table 1
The rheological parameters obtained by Power-law and Cross-empirical equations for XG at different temperatures and salinities. $c_{XG} = 1750$ mg·L^{-1}.

T, °C	c_{NaCl}, mg·L^{-1}	k	n	η_0, mPa·s	η_∞, mPa·s	$\dot{\gamma}_b$	m
25	0	0.53	0.25	2022	8.3	0.11	1.12
55	0	0.21	0.39	790	6.1	0.07	0.87
75	0	0.14	0.48	364	5.6	0.03	0.81
25	5000	0.33	0.32	1250	7.6	0.10	1.01
25	10,000	0.32	0.33	1241	7.6	0.09	1.01

$$G' = G_0 \frac{\omega^2 \tau_R^2}{1 + \omega^2 \tau_R^2} \tag{3}$$

$$G'' = G_0 \frac{\omega \tau_R}{1 + \omega^2 \tau_R^2} \tag{4}$$

where G_0 is the plateau modulus, ι_R is the relaxation time, the radian frequency $\omega = 2\pi f$, and f is the frequency in Hertz.

As shown in Fig. 7(a), for pure aqueous XG solution at 25 °C, the

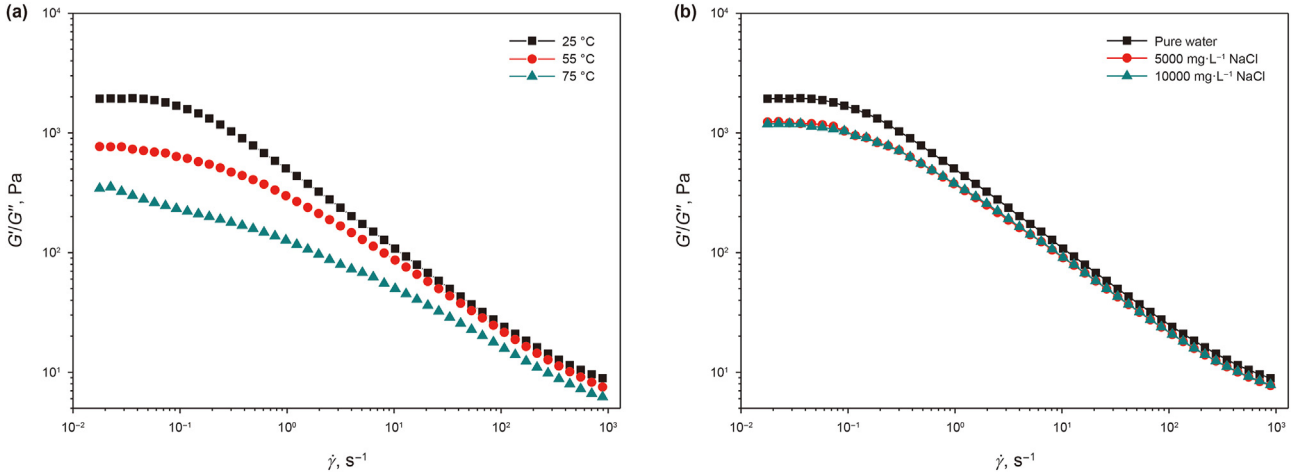

Fig. 6. The dependence of the apparent viscosity (η) of pure aqueous XG solution on the shear rate at (**a**) different temperatures in pure water and (**b**) different salinities at 25 °C. $c_{XG} = 1750$ mg·L^{-1}..

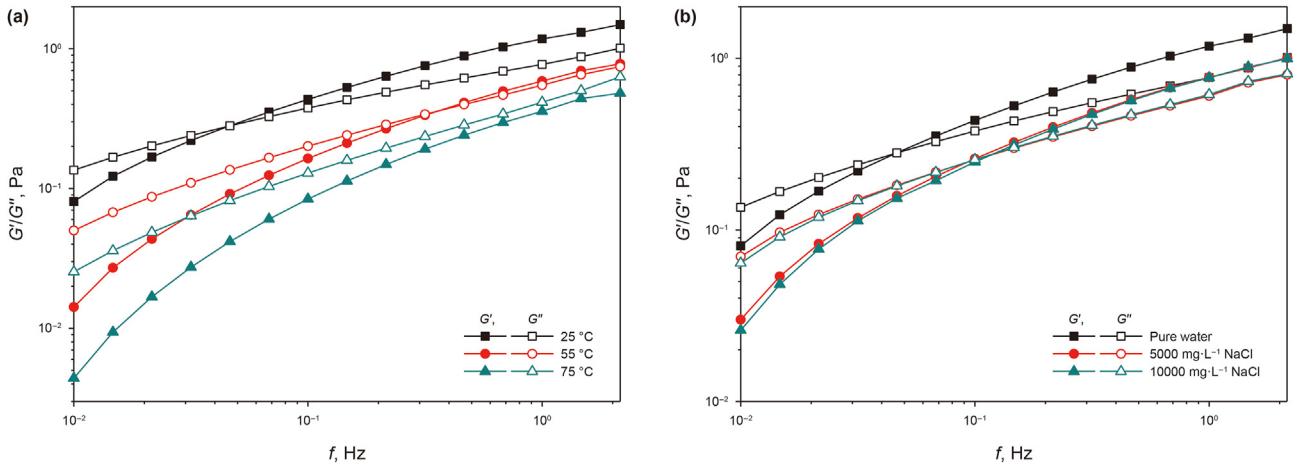

Fig. 7. The frequency dependence of the storage modulus (G', solid data points) and loss modulus (G'', hollow data points) of pure aqueous XG solution at (**a**) different temperatures and (**b**) different salinities at 25 °C. c_{XG} = 1750 mg·L^{-1}..

elasticity is the main factor in the viscoelasticity ($G' > G''$), indicating that a weak gel-like structure is formed. At a higher temperature, the dynamic modulus of the XG solution obviously decreased. At 75 °C, in the experimental frequency range, a disordered molecular coil structure within the XG solution because of $G' < G''$. Heating destroys the network structure of XG and results in the solution more viscous. Fig. 7(b) shows that G' and G'' of the XG solution are reduced in NaCl solutions but slightly decreases at higher salinity, which was consistent with the results reported by Wang et al. (2002). At 10,000 mg·L^{-1}, the XG solution is more elastic ($G' > G''$) in half of the experimental frequency range, indicating that some network structures still exist.

In aqueous XG solutions, when the solution regime transits from a dilute state to a semidilute state, the molecular conformation of XG transforms from a coil to helix simultaneously. Because of the steric effect of trisaccharide side chains and the self-association of molecules, irregular double helices are always formed for XG molecules (Xu et al. 2013, 2015). However, the aggregate structure formed by XG molecules is just a transient network formed by hydrogen bonds dependent on the temperature (Modig et al., 2003; Tako et al., 2009). Moreover, high temperature also weakens the van der Waals force by accelerating the motion of the molecules. Consequently, the aggregate structure of XG is easily dissociated at high temperature.

Due to the negative charge of XG, the counterions in the aqueous solution always screen the electrostatic repulsion between the XG molecular chains. Thus, the XG molecular structure collapse and chains fold up (Li et al., 2017). The molecular conformation of XG in pure water is in the stretched state; when NaCl is added, the hydrodynamic size of the XG molecular aggregate is compressed by Na^+. However, the molecules of XG still maintain a double helix at higher salinity due to the semirigid chains. Therefore, it can be thought that, compared with the salinity provided by NaCl, the molecular structure of XG is more dependent on the temperature.

3.3. Rheology of XG/AANP hybrid dispersions

In the presence of 10,000 mg/L NaCl at 75 °C, the η of the XG/nanosilica hybrid dispersion is higher than that of XG solution or nanosilica dispersion at the same concentration, as shown in Fig. 8. In particular, the viscosity increases more for the combination of XG and AANP than for the combination of XG and NP. The hydrogen bonds between the hydroxyl groups of XG and the silanol of NP are the main role for the interaction between XG and NP. However, for

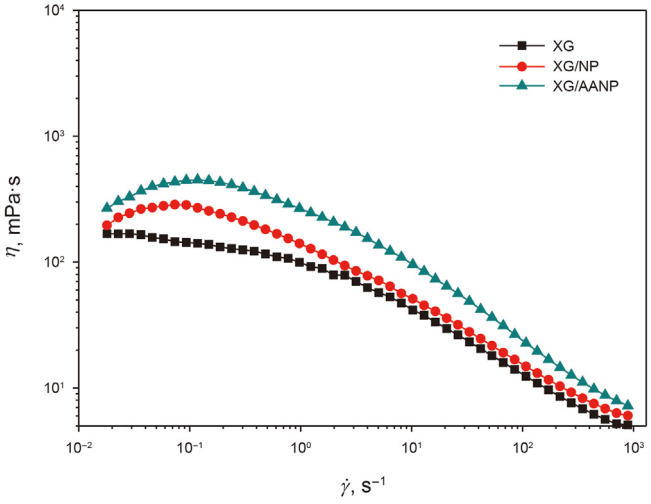

Fig. 8. The dependence of the apparent viscosity (η) of aqueous XG/nanosilica hybrid dispersions on the shear rate. c_{XG} = 1750 mg·L^{-1}, $c_{NP,\ AANP}$ = 0.8 wt%, c_{NaCl} = 10,000 mg·L^{-1}, T = 75 °C.

the interaction between XG and AANP, the hydrogen bonds were further strengthened by amides grafted on the nanosilicas. Meanwhile, the hydrophobic interaction between alkyl chains of AANPs and methyl groups located in the side chains of XG makes a substantial contribution at high temperature and high salinity.

For the lone XG solution, the flow curve for η with respect to $\dot{\gamma}$ contains two parts: the Newtonian fluid stage ($\dot{\gamma} < 0.05$ s^{-1}) and shear-thinning stage ($\dot{\gamma} > 0.05$ s^{-1}). The XG molecular aggregates dissociate into disordered coils when the critical shear stress is reached (Xu et al., 2015). However, for the XG/nanosilica hybrid dispersion, a different shear behavior phenomenon was found: shear thickening in the initial shearing stage, meaning that an optimal shear rate ($\dot{\gamma}_o$) exists. The values of $\dot{\gamma}_o$ for XG/NP and XG/AANP are 0.07 s^{-1} and 0.12 s^{-1}, respectively. When nanosilicas are grafted with amide and alkyl groups, the mobility in the dispersion becomes slow. Appropriate shear forces can promote the nanosilicas move to a position with more contact with XG molecular chains, a maximum viscosity appears as a result.

The rheological parameters fitted by Power-law and Cross-empirical equations for XG/nanosilicas in the presence of 10,000 mg/L NaCl at 75 °C are shown in Table 2. All values of n are

Table 2
The rheological parameters obtained by Power-law and Cross-empirical equation for XG/nanosilicas. c_{XG} = 1750 mg·L^{-1}, $c_{NP,\ AANP}$ = 0.8 wt%, c_{NaCl} = 10,000 mg·L^{-1}, T = 75 °C.

Systems	k	n	η_0, mPa·s	η_∞, mPa·s	$\dot{\gamma}_b$	m
XG	0.10	0.51	172	5.0	0.04	0.79
XG/NP	0.15	0.46	203	6.0	0.13	0.82
XG/AANP	0.19	0.41	260	7.2	0.22	0.87

less than 1, indicating that XG/nanosilica dispersions are also pseudoplastic fluids. With the addition of nanosilicas, the values of k, η_0, η_∞, $\dot{\gamma}_b$ and m of XG are enhanced. Moreover, these values of XG/AANP dispersion are higher than those of the XG/NP dispersion, while the values of n are lower.

Aqueous XG/nanosilica dispersions in the presence of 10,000 mg/L NaCl are sheared at the rate of 0.1 s^{-1} and 75 °C for 60 min, as shown in Fig. 9. With increasing shearing time, the viscosities of XG solutions with and without nanosilicas decrease in the early shear process. However, for XG solution alone, the viscosity is essentially unchanged when the shearing time exceeds 15 min. For XG/nanosilicas, the dispersions exhibit a phenomenon of first decrease and then increase on the viscosity. Moreover, the shearing time when the viscosity starts to rise of the XG/AANP dispersion (9.7 min) is earlier than that of the XG/NP dispersion (20 min). After 60 min of shearing, the viscosity retention rates of the XG, XG/NP and XG/AANP dispersions are 61.9%, 92.7% and 115%, respectively. The results indicate that the addition of nanosilicas improves the shear resistance of XG solutions. As the XG molecular chains are dispersed during the shearing process, the nanosilicas between the molecular chains are also evenly rearranged, which increases the force between the XG molecular chains and the nanosilicas, and a compact network chain is formed for the XG/nanosilica hybrids. In addition, because AANP carries amides and alkyls on the surface, these groups contact and entangle with the XG molecular chain, forming larger size aggregates. Therefore, the XG/AANP hybrids exhibit viscosity-increasing performance with shear time.

The dynamic moduli of the XG solution increases by adding NPs or AANPs in the presence of 10,000 mg·L^{-1} NaCl at 75 °C, as shown in Fig. 10. For the XG/NP hybrids, $G'' > G'$ and a strong dependence of dynamic moduli on the frequency indicate that a disordered

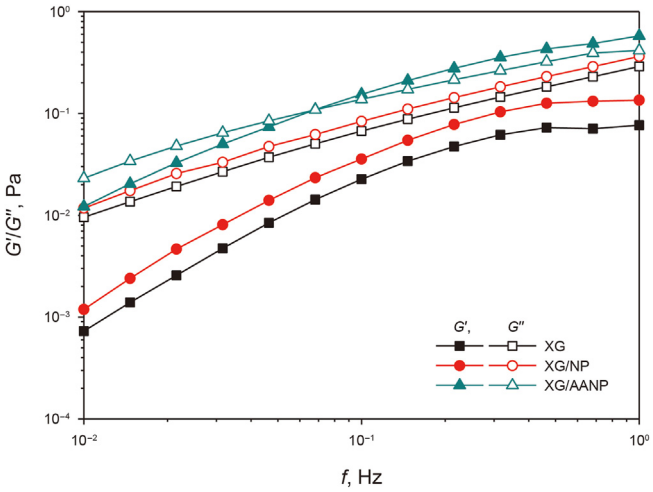

Fig. 10. The dependence of the storage modulus (G', solid data points) and loss modulus (G'', hollow data points) of aqueous XG/nanosilica hybrid dispersions on the oscillation frequency. c_{XG} = 1750 mg·L^{-1}, $c_{NP,\ AANP}$ = 0.8 wt%, c_{NaCl} = 10,000 mg·L^{-1}, T = 75 °C.

structure formed. For the XG/AANP hybrids, $G' > G''$ over half of the range of oscillation frequency values, and some network structures reform within the dispersion. Furthermore, G' and G'' of the XG/AANP hybrid are higher than those of the XG/NP hybrid. The results indicate that AANPs effectively reconnect the dispersed molecular coils of XG at high temperature and high salinity.

3.4. Dependence of the rheology on the component concentration

In the presence of 10,000 mg·L^{-1} NaCl at 75 °C, with increasing the XG concentration, the apparent viscosity ($\eta_{0.1}$) of the XG/AANP hybrid dispersion rapidly increases, while that of the lone XG solution slowly increases, as shown in Fig. 11. This means that AANP can significantly improve the temperature tolerance and salt tolerance of XG/AANP hybrid systems. At higher concentrations of XG, XG molecules are not fully saturated with nanosilicas. The self-aggregation between XG molecules gradually increased. The XG

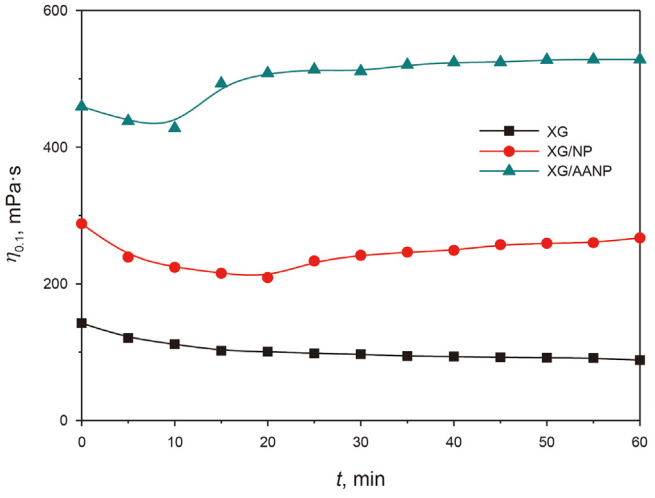

Fig. 9. The dependence of the apparent viscosity ($\eta_{0.1}$) of aqueous XG/nanosilica hybrid dispersions on the shear time. c_{XG} = 1750 mg·L^{-1}, $c_{NP,\ AANP}$ = 0.8 wt%, c_{NaCl} = 10,000 mg·L^{-1}, T = 75 °C.

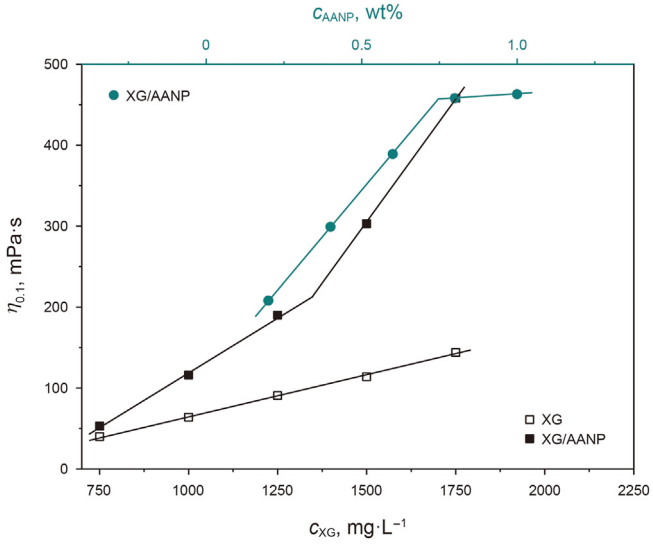

Fig. 11. The apparent viscosity ($\eta_{0.1}$) of aqueous XG/AANP hybrid dispersions at different XG concentrations (c_{AANP} = 0.8 wt%) and AANP concentrations (c_{XG} = 1750 mg·L^{-1}). c_{NaCl} = 10,000 mg·L^{-1}, T = 75 °C.

concentration was fixed at 1750 mg·L^{-1}, when the concentration of AANP exceeds 0.74 wt%, the $\eta_{0.1}$ of the XG/AANP hybrid dispersion slightly increases. It was thought that nearly all molecular chains of XG at 1750 mg·L^{-1} are connected by AANPs at 0.74 wt%. Optimal concentrations exist for XG and AANP to form the NP-polysaccharide hybrid that significantly improving the rheology.

For the particulate gels, the background fluid mainly contributes to the viscous part, while the network skeleton structure cross-linked by particles acts as elastic part (Trappe and Weitz, 2000). It was reported by Oh et al. (1999) that, at dilute concentrations and 25 °C, XG alone did not exhibit weak gel behavior, and the nanoslics mediated the gel structure. At a concentrated concentration of XG (10,000 mg·L^{-1}), the solution alone exhibited weak gel structure, and the nanoslics further enhanced the strength of the gel. At 10,000 mg·L^{-1} NaCl and 75 °C, $G' > G''$ when the concentrations of XG and AANP are 1750 mg·L^{-1} and 0.74 wt%, respectively, as shown in Fig. 12, indicating that some network structures were formed for the XG/AANP hybrid system. A weak gel formed over time for 5000 mg·L^{-1} LBG at high nanosilica concentration (20%) (Oliveira et al., 2010). Compared with the LBG/NP hybrid, XG gelation requires less loading per concentration unit of AANP, which is due to the strong interaction between AANP and XG.

3.5. Dependence of the rheology on the temperature

When heating from 25 °C to 75 °C, a conformation transition occurs for the XG molecules. To check the temperature tolerance of the XG/AANP hybrid dispersions, the thermal sensitivity of the apparent viscosity ($\eta_{0.1}$) in the presence of inorganic salt was investigated. The viscosity retention rate (φ) of XG/nanosilica hybrid dispersions at different temperatures is given in Fig. 13. As the temperature increases, the values of φ gradually decrease, and the XG and XG/nanosilica hybrid dispersions show thermothinning behavior at 10,000 mg·L^{-1} NaCl. However, the viscosity reduction of XG alone is more than that of XG/nanosilica hybrids. The addition of nanosilicas delays the reduction of XG viscosity retention, and the XG/AANP hybrid dispersion has a greater φ than the XG/NP hybrid or single XG at the same temperature. At 75 °C, the φ values of the XG, XG/NP hybrid and XG/AANP hybrid are 13.7%, 25.0% and 32.9%, respectively. Therefore, nanosilicas improve temperature sensitivity of XG solution. At higher temperatures, the G' and G'' values of XG/AANP hybrid are still higher than those of XG alone or the XG/NP hybrid, as shown in Fig. 14. At 75 °C, XG/AANP hybrid dispersion shows predominantly elasticity property ($G' > G''$), meaning that the network structure of the XG/AANP hybrid still remains at 75 °C and 10,000 mg·L^{-1} NaCl.

Heating accelerates the motion of the molecules and weakens the van der Waals forces and hydrogen bonds (Zhang et al., 2019). Substantial hydrogen bond distortions at higher temperature are responsible for the gradual loss of second-neighbor spatial correlations. At high temperature, the water molecules that adhered to the molecular chains tend to escape because of the weakening of the hydrogen bonds and the thermal motion of the molecules. For XG alone, heating breaks down molecular associations that are mainly formed by hydrogen bonds. Consequently, the transient network structures of XG are destroyed easily at high temperature due to the entanglement of molecular chains with a finite lifetime. Therefore, the temperature sensitivity of XG stems from the determined effect on the lifetime of the bonds by the temperature.

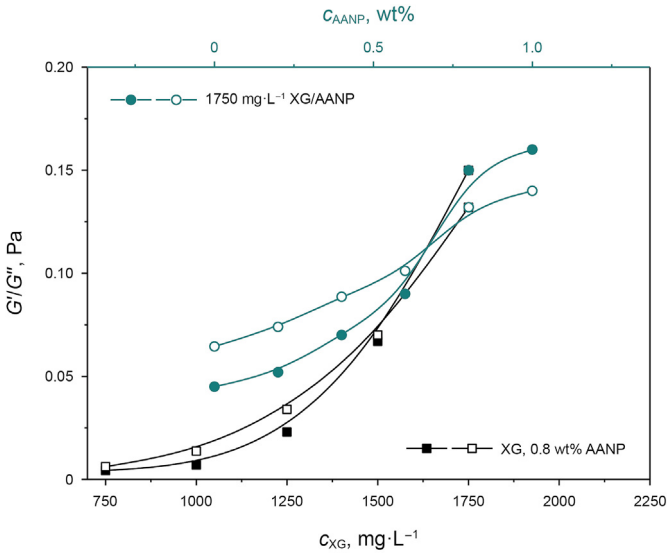

Fig. 12. At the frequency of 0.1 Hz, the G'(solid data points) and G'' (hollow data points) of aqueous XG/AANP hybrid dispersions at different XG concentrations (c_{AANP} = 0.8 wt%) and AANP concentrations (c_{XG} = 1750 mg·L^{-1}). c_{NaCl} = 10,000 mg·L^{-1}, T = 75 °C.

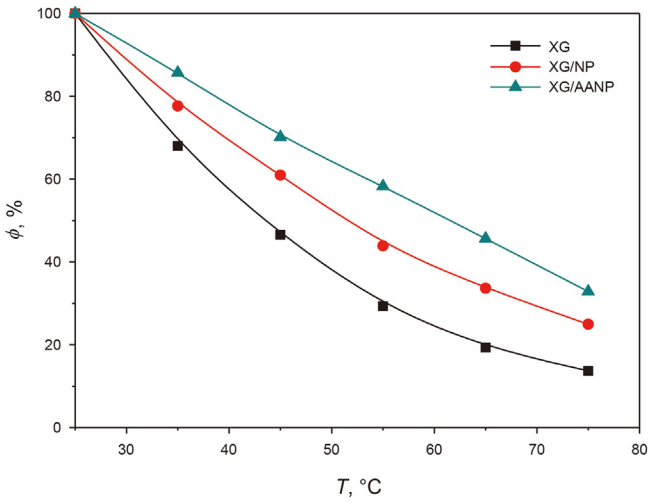

Fig. 13. The viscosity retention rate (φ) of aqueous XG/nanosilica hybrid dispersions at different temperatures. c_{XG} = 1750 mg·L^{-1}, $c_{NP,\ AANP}$ = 0.8 wt%, c_{NaCl} = 10,000 mg·L^{-1}..

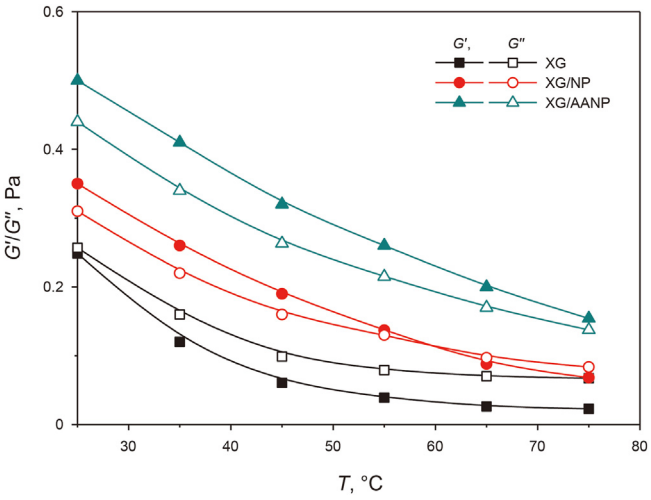

Fig. 14. The dependence of the storage modulus (G', solid data points) and loss modulus (G'', hollow data points) of aqueous XG/nanosilica hybrid dispersions on the temperature. c_{XG} = 1750 mg·L^{-1}, $c_{NP,\ AANP}$ = 0.8 wt%, c_{NaCl} = 10,000 mg·L^{-1}..

For XG/nanosilica hybrids, some hydrogen bonds are impaired as the temperature increases. The viscosity reduction is due to the disassociation of the network junctions and the binding of nanosilicas to XG. However, the $\eta_{0.1}$ and dynamic moduli of XG/AANP remain higher than those of the lone XG solution and XG/NP hybrid dispersion at the same temperature. The improvement against heating of the hybrid could be interpreted in terms of the physical crosslinking of XG macromolecular chains with the AANPs. This interaction appears to have stabilized the helical XG structure, delaying the helix-coil conformational transition to a higher temperature. In addition to the hydrogen bond, the attraction between alkyl groups of AANPs and methyl of XG reinforces the network structures of XG and promotes the formation of hybrid networks. Moreover, the heat resistance of the hydrophobic force between alkyls is stronger than that of hydrogen bonds. These interactions reinforce the network structures of XG and improve the thermal stability of hybrids.

3.6. Dependence of the rheology on the inorganic salts

Generally, the electrostatic repulsion between polyelectrolyte molecules is constantly screened by counterions, causing the molecular chains to curl up (Wyatt et al., 2011). XG is a polyelectrolyte with a negative charge. As known before, the viscoelasticity of pure aqueous XG solution is slightly influenced by the salinity when the concentration of NaCl exceeds 5000 mg·L^{-1} at 25 °C. However, the changes of circumstances at high temperature have not been yet understood. Therefore, the rheological behaviors of XG dispersions with and without nanosilicas at different salinities and inorganic salts were investigated.

Fig. 15 and Fig. 16 show that the steady-state shear and dynamic oscillation of XG/nanosilica hybrid dispersions at 75 °C and different salinities. As the concentration of NaCl increases from 5000 mg·L^{-1} to 100,000 mg·L^{-1} at 75 °C, $\eta_{0.1}$, G' and G'' of the XG solution gradually decreased, which is different from its rheological behavior at 25 °C. However, at 75 °C, nanosilicas improve the rheology of XG dispersions, and the $\eta_{0.1}$, G' and G'' of the XG/AANP hybrid are higher than those of XG alone or the XG/NP hybrid at the same salinity. When the salinity reaches 100,000 mg·L^{-1} at 75 °C, the XG/AANP dispersion shows predominantly elastic properties ($G' > G''$). Although high temperature weakens the salt tolerance of XG, AANPs effectively improve this disadvantage. The nanosilica possesses negative charges and a portion of cations adsorb on the nanosilica surface. Thereby, the electrostatic shielding effect of counterions on the molecular repulsion of XG is greatly weakened. The molecular configuration of XG is stretched and recovered to a certain extent as a result. However, for the XG/NP hybrid, the dissociation of silanol groups from nanosilicas reduces the number of −OH groups available for hydrogen bonds with XG. Hence, the interaction between XG and NP becomes weak. For the XG/AANP hybrid, based on the partially stretched configuration of XG, the improved surface alkyl chains and amide groups of nanosilicas effectively mediate the polysaccharide chains to further form a network structure.

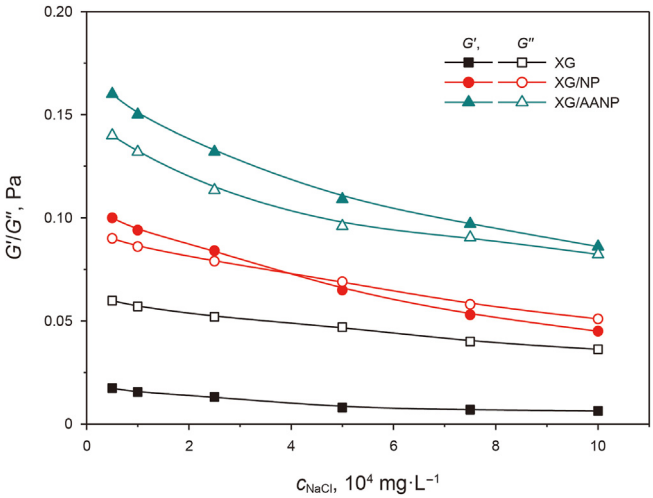

Fig. 16. The dependence of the storage modulus (G', solid data points) and loss modulus (G'', hollow data points) of aqueous XG/nanosilica hybrid dispersions on salinity. c_{XG} = 1750 mg·L^{-1}, $c_{NP,\ AANP}$ = 0.8 wt%, T = 75 °C.

The changes in $\eta_{0.1}$ of the XG/nanosilica hybrid dispersions in different inorganic salts (NaCl, $CaCl_2$ and $MgCl_2$) are shown in Fig. 17. Under the same salinity (10,000 mg·L^{-1}), the $\eta_{0.1}$ of the XG solution with $CaCl_2$ or $MgCl_2$ is lower than that with NaCl. Under the same inorganic salt concentration, the ionic strength of the divalent salt is higher, and the charge shielding effect is stronger. The gel-like formed by the XG solution is more easily compressed as a result. In different brines, the $\eta_{0.1}$ of the XG/NP dispersion is slightly higher than that of the XG solution, but the difference is not

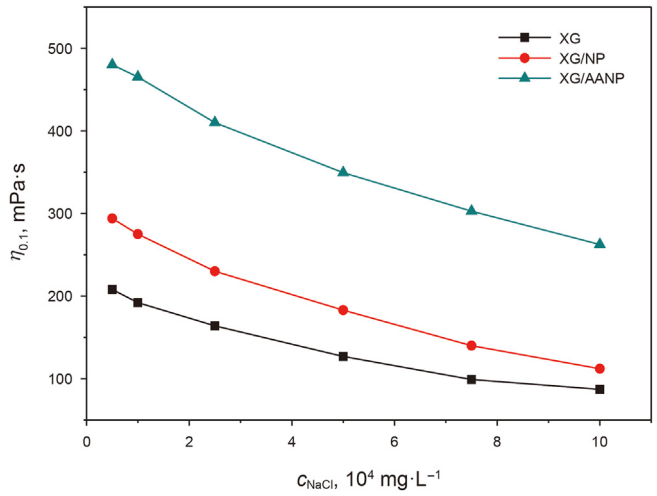

Fig. 15. The dependence of the apparent viscosity ($\eta_{0.1}$) of aqueous XG/nanosilica hybrid dispersions on salinity. c_{XG} = 1750 mg·L^{-1}, $c_{NP,\ AANP}$ = 0.8 wt%, T = 75 °C.

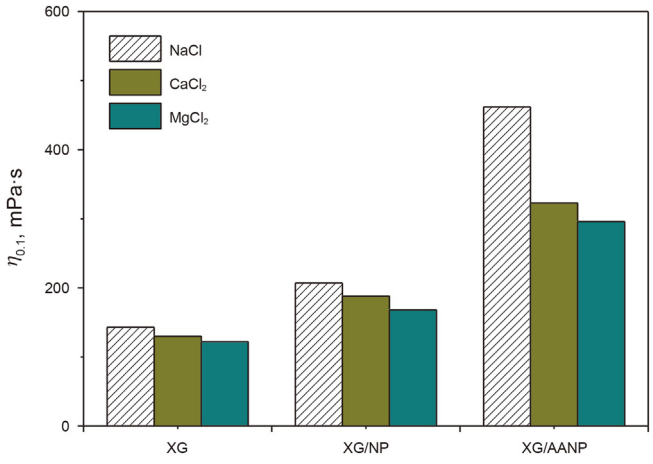

Fig. 17. The apparent viscosity ($\eta_{0.1}$) of aqueous XG/AANP hybrid dispersions with different inorganic salts (NaCl, $CaCl_2$ and $MgCl_2$). c_{XG} = 1750 mg·L^{-1}, $c_{NP,\ AANP}$ = 0.8 wt %, c_{salt} = 10,000 mg·L^{-1}, T = 75 °C.

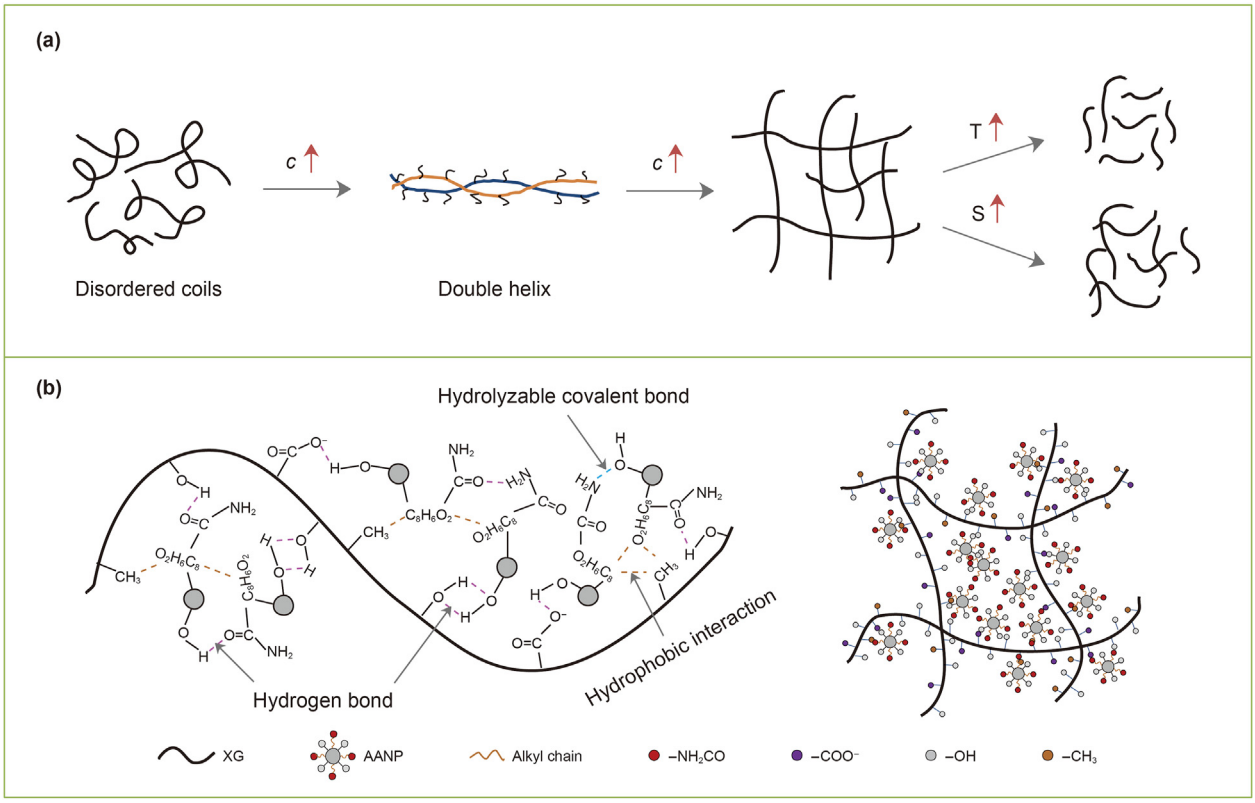

Fig. 18. Schematic representation for (**a**) molecular configuration changes of XG and (**b**) the interaction between XG and AANP. *c*: concentration, T: temperature, S: salinity.

much. NPs adsorbed on the XG molecular chains thicken the hydration layer and weaken the charge shielding effect of the inorganic salt on the XG molecular aggregation structure. However, because the degree of cross-linking of NP and XG molecular chains is weak, it is not enough to resist the deformation of the aggregate structure caused by high salinity. For the XG/AANP hybrid, $\eta_{0.1}$ is 3.2, 2.5 and 2.4 times that of the single XG solution in NaCl, $CaCl_2$ and $MgCl_2$ solutions, respectively. AANPs with alkyl chains and amide groups have a strong cross-linking and entanglement effect with the XG molecular chain, which obviously improves the salt tolerance of the XG molecular aggregate structure, especially for monovalent inorganic salts.

3.7. Synergy mechanism of XG and AANP on thickening at high temperature and high salinity

At 25 °C, the molecular structure of XG in a dilute pure aqueous solution presents a state of disordered coils and becomes a double helix structure in a concentrated solution. The intermolecular associations of XG occur between the methyl and the counter hemiacetal on different molecules via van der Waals forces and between the side and backbone chains by hydrogen bonds (Morris et al., 1996). Meanwhile, hydroxyl, carboxyl and carbonyl centers in XG molecules establish hydrogen bonds with the adsorbed water. When heated from 25 °C to 75 °C, the XG molecular conformation transforms from helix to coil (Sato et al., 1984). For the conformation transition of XG in saltwater, such as NaCl and $CaCl_2$, XG molecules tend to take an ordered conformation (Rochefort and Middleman, 1987 . Mohammed et al., 2007). Inorganic cations compact the hydrated layer around long-chain molecules by dipolar interactions. However, they have limited influence on the water molecules wrapped in the core of the XG double helix at low temperature. When the temperature rises, the water molecules that adhered to the core of the double helix gradually break away, causing the double helix to lose the support of the internal bound water. Then, the double-helical conformation is further compressed by the screening effect of inorganic salts.

For the gel-like structure formation of XG in the presence of nanosilicas, it is thought that the semiflexible XG molecules adsorbed onto the nanosilicas surface interpenetrate into the adsorbed layers of the neighboring ones. The molecular conformation of the XG/NP hybrid was destroyed by counterions (Na^+ and Ca^{2+}) at high temperature (75 °C). As mentioned before, the bare NPs distribution in an aqueous solution is not homogeneous, agglomeration always occurs, and obvious precipitates can even be observed in the lower part of the solution. For AANPs, the amide group can improve the dispersibility of particles, increasing the chance of contact with macromolecules when combined with XG. As shown in Fig. 18, the XG molecular chains adopt a stretched configuration based on the double helix primary structure. AANPs form aggregates around the XG molecular chains with a larger hydrodynamic size which was verified in Table 3. The molecular chains of XG act as templates for particle gathering, resulting in a particle cross-linked network. AANP clusters hinder the mobility of XG molecules and enhance junction zones within the network. The molecular network of XG was reinforced by AANP clustering, in addition to conventional hydrogen bonds, it also was attributed to the hydrophobic attraction between the methyl groups of XG and alkyl chains of AANP. The AANPs reduce the electrostatic shielding effect of counterions on the molecular conformation of XG due to the same charge. Additionally, AANPs increase the rigidity of the network by filling the XG molecular chain cavities with the appropriate size. This plays a positive role in inhibiting the network structure collapse of the lone XG caused by high temperature and

Table 3
Molecular hydrodynamic length (L) and zeta potential (ξ) of XG with and without nanosilicas.

Composition					L, nm	ξ, mV
XG, mg·L^{-1}	NP, wt%	AANP, wt%	NaCl, mg·L^{-1}	T, °C		
1750	0	0	0	25	807	−44.3
1750	0	0	0	75	550	−55.7
1750	0	0	10,000	25	692	−16.2
1750	0	0	10,000	75	340	−22.8
1750	0.8	0	10,000	75	439	−25.1
1750	0	0.8	10,000	75	531	−27.9

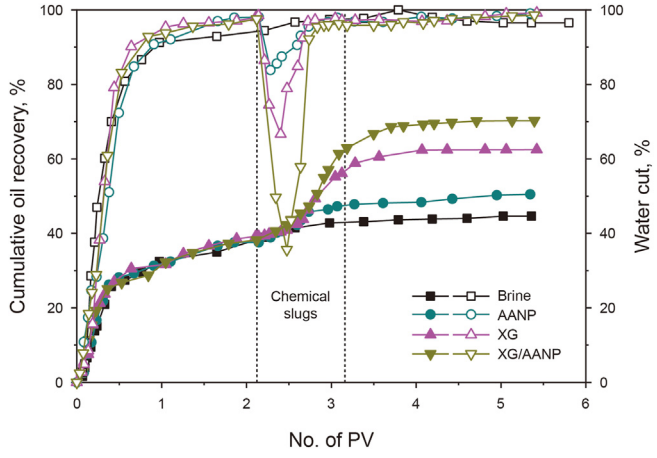

Fig. 19. Oil recovery efficiency (solid) and water cut (hollow) as a function of No. of PV for different systems at 75 °C and 10,000 mg·L^{-1} salinity.

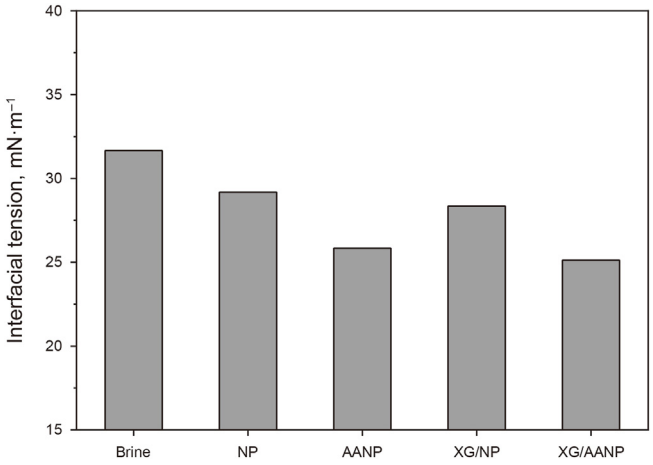

Fig. 20. Interfacial tension between different systems and crude oil at 75 °C and 10,000 mg·L^{-1} salinity.

high salinity. Consequently, the further interactions of XG-AANP and AANP-AANP are mainly responsible for the improved rheological behavior on the temperature/salt tolerance.

3.8. Oil recovery efficiency and mechanism

The oil recovery efficiency of XG/AANP hybrid under reservoir conditions of 75 °C and of 10,000 mg·L^{-1} NaCl was shown in Fig. 19. During the initial waterflooding, the cumulative oil recovery increases rapidly and produces more oil. Due to the existence of the viscosity fingering effect, when the waterflooding progresses to a certain extent, water channeling occurs, the oil displacement efficiency reduces, and the cumulative oil recovery slowly increase. After switching to chemical flooding, the oil-water mobility ratio decreases, the occurrence of fingering is inhibited, and the oil recovery efficiency is greatly improved. As shown in Table 4, XG/AANP recovers approximately 18.5% more OOIP (original oil in place) than AANP and 11.3% more OOIP than XG. The minimum water cuts of AANP, XG and XG/AANP are 84.0%, 66.4% and 35.4%, respectively. The XG/AANP hybrid is more efficient than the XG in decreasing the water cut.

The mechanism for EOR mainly includes increasing sweep volume and improving oil washing efficiency (Xu et al., 2014; Hou et al., 2015). Fig. 20 shows the interfacial tension between different oil displacing agents and crude oil. Though the interfacial tension (25.1 mN·m^{-1}) of XG/AANP is lower than that (28.4 mN·m^{-1}) of XG/NP. However, the interfacial tension between XG/AANP and crude oil has not achieved an ultra-low level, the oil-water interface activities are not enhanced by the XG/AANP hybrid. Combining the results of viscosity and interfacial tension, it can be inferred that the high oil recovery efficiency of XG/AANP is mainly due to the higher bulk viscosity which can effectively improve the oil-water mobility ratio and expand the displacement coefficient. And oil-water interfacial tension only provides a small contribution for EOR.

4. Conclusions

Nanosilicas with alkyl and amide groups were synthesized and used to improve the rheology of XG solution on temperature/salt tolerance. The rheology of XG solution obviously changed at 75 °C and 10,000 mg·L^{-1} NaCl. A significant synergy occurs for the combination of XG and AANPs had on improving the rheological properties at high temperature and high salinity. Optimal component concentrations exist for XG and AANP to interact with the best

Table 4
Summary of flooding tests.

System	Porosity, %	Permeability, μm^2	Initial oil saturation, %	Waterflooding recovery, %OOIP	Tertiary recovery, %OOIP	Final recovery, %OOIP
Brine	41.6	1.42	83.1	44.5	–	44.5
AANP	44.5	1.24	81.7	39.3	11.0	50.3
XG	42.9	1.78	84.2	40.2	22.3	62.5
XG/AANP	42.7	1.31	82.5	41.0	29.5	70.5

synergistic effect. At 75 °C and 10,000 mg·L^{-1} NaCl, the XG/AANP hybrid dispersion show predominantly elastic properties. The molecular chains of XG act as templates for particle gathering, resulting in a particle cross-linked network. AANP clusters hinder the mobility of XG molecules and enhance junction zones within the network. For the interaction between XG and AANP, the hydrogen bonds were further strengthened by amides grafted on the nanosilicas. Meanwhile, a substantial contribution was made by the hydrophobic interaction between alkyl chains of AANPs and methyl groups located in the side chains of XG at high temperature and high salinity. The AANPs effectively increase the efficiency of XG for EOR under the reservoir conditions. The EOR mechanism of the XG/AANP hybrid is mainly attributed to the synergistic thickening. It is an effective strategy to improve the EOR of XG by introducing nanosilicas modified with alkyl chains and amide groups.

Acknowledgements

We gratefully acknowledge financial supports from the Major Program of National Natural Science Foundation of China (Grant No. 42090024), the National Natural Science Foundation of China (Grant No. 52004322) and the Natural Science Foundation of Shandong Province, China (Grant No. ZR2020QE108).

References

Edward, J.T., 1970. Molecular volumes and the Stokes-Einstein equation. J. Chem. Educ. 47 (4), 261. https://doi.org/10.1021/ed047p261.

Balazs, A.C., Emrick, T., Russell, T.P., 2006. Nanoparticle polymer composites: where two small worlds meet. Science 314 (5802), 1107. https://doi.org/10.1126/science.1130557.

Batista, C.A., Larson, R.G., Kotov, N.A., 2015. Nonadditivity of nanoparticle interactions. Science 350 (6257), 1242477. https://doi.org/10.1126/science.1242477.

Cheng, S., Xie, S.J., Carrillo, J.Y., et al., 2017. Big effect of small nanoparticles: a shift in paradigm for polymer nanocomposites. ACS Nano 11 (1), 752–759. https://doi.org/10.1021/acsnano.6b07172.

Coradin, T., Bah, S., Livage, J., 2004. Gelatine/silicate interactions: from nanoparticles to composite gels. Colloids Surf., B 35 (1), 53–58. https://doi.org/10.1016/j.colsurfb.2004.02.008.

Daniel-da-Silva, A.L., Bordado, J.C.M., Martín-Martínez, J.M., 2008. Moisture curing kinetics of isocyanate ended urethane quasi-prepolymers monitored by IR spectroscopy and DSC. J. Appl. Polym. Sci. 107 (2), 700–709. https://doi.org/10.1002/app.26453.

De Jong, S., Van de Velde, F., 2007. Charge density of polysaccharide controls microstructure and large deformation properties of mixed gels. Food Hydrocolloids 21 (7), 1172–1187. https://doi.org/10.1016/j.foodhyd.2006.09.004.

Gilbert, L., Loisel, V., Savary, G., et al., 2013. Stretching properties of xanthan, carob, modified guar and celluloses in cosmetic emulsions. Carbohyd Polym 93 (2), 644–650. https://doi.org/10.1016/j.carbpol.2012.12.028.

Gregory, J., Barany, S., 2011. Adsorption and flocculation by polymers and polymer mixtures. Adv Colloid Interfac 169 (1), 1–12. https://doi.org/10.1016/j.cis.2011.06.004.

Habibpour, M., Clark, P.E., 2017. Drag reduction behavior of hydrolyzed polyacrylamide/xanthan gum mixed polymer solutions. Petrol. Sci. 14 (2), 412–423. https://doi.org/10.1007/s12182-017-0152-7.

Hou, B., Wang, Y., Huang, Y., 2015. Mechanistic study of wettability alteration of oil-wet sandstone surface using different surfactants. Appl. Surf. Sci. 330, 56–64. https://doi.org/10.1016/j.apsusc.2014.12.185.

Hu, Z., Haruna, M.A., Gao, H., et al., 2017. Rheological properties of partially hydrolyzed polyacrylamide seeded by nanoparticles. Ind. Eng. Chem. Res. 56 (12), 3456–3463. https://doi.org/10.1021/acs.iecr.6b05036.

Kennedy, J.R., Kent, K.E., Brown, J.R., 2015. Rheology of dispersions of xanthan gum, locust bean gum and mixed biopolymer gel with silicon dioxide nanoparticles. Mater. Sci. Eng., C 48, 347–353. https://doi.org/10.1016/j.msec.2014.12.040.

Koenderink, G.H., Sacanna, S., Aarts, D.G., et al., 2004. Rotational and translational diffusion of fluorocarbon tracer spheres in semidilute xanthan solutions. Phys. Rev. E 69 (2), 021804. https://doi.org/10.1103/PhysRevE.69.021804.

Li, Y., Xu, L., Gong, H., et al., 2017. A microbial exopolysaccharide produced by Sphingomonas species for enhanced heavy oil recovery at high temperature and high salinity. Energy Fuel. 31 (4), 3960–3969. https://doi.org/10.1021/acs.energyfuels.6b02923.

Mao, C.F., 2008. Self- and cross-associations in two-component mixed polymer gels. J. Polym. Sci., Polym. Phys. Ed. 46 (1), 80–91. https://doi.org/10.1002/polb.21344.

Maruyama, Y., Mikami, B., Hashimoto, W., et al., 2007. A structural factor responsible for substrate recognition by Bacillus sp. GL1 xanthan lyase that acts specifically on pyruvated side chains of xanthan. Biochemistry 46 (3), 781–791. https://doi.org/10.1021/bi0619775.

Modig, K., Pfrommer, B.G., Halle, B., 2003. Temperature-dependent hydrogen-bond geometry in liquid water. Phys. Rev. Lett. 90 (7), 075502. https://doi.org/10.1103/PhysRevLett.90.075502.

Mohammed, Z.H., Haque, A., Richardson, R.K., et al., 2007. Promotion and inhibition of xanthan 'weak-gel' rheology by calcium ions. Carbohydr. Polym. 70 (1), 38–45. https://doi.org/10.1016/j.carbpol.2007.02.026.

Moreira, A.S., Coimbra, M.A., Nunes, F.M., et al., 2011. Evaluation of the effect of roasting on the structure of coffee galactomannans using model oligosaccharides. J. Agric. Food Chem. 59 (18), 10078–10087. https://doi.org/10.1021/jf2021072.

Morris, E., Gothard, M., Hember, M., et al., 1996. Conformational and rheological transitions of welan, rhamsan and acylated gellan. Carbohydr. Polym. 30 (2), 165–175. https://doi.org/10.1016/S0144-8617(96)00059-8.

Mu, J.H., Li, G.Z., Jia, X.L., et al., 2002. Rheological properties and microstructures of anionic micellar solutions in the presence of different inorganic salts. J. Phys. Chem. B 106 (44), 11685–11693. https://doi.org/10.1021/jp014096a.

Oh, M.H., So, J.H., Yang, S.-M., 1999. Rheological evidence for the silica-mediated gelation of xanthan gum. J. Colloid Interface Sci. 216 (2), 320–328. https://doi.org/10.1006/jcis.1999.6325.

Oliveira, F., Monteiro, S.R., Barros-Timmons, A., Lopes-da-Silva, J., 2010. Weak-gel formation in dispersions of silica particles in a matrix of a non-ionic polysaccharide: structure and rheological characterization. Carbohydr. Polym. 82 (4), 1219–1227. https://doi.org/10.1016/j.carbpol.2010.06.046.

Pashkovski, E.E., Masters, J.G., Mehreteab, A., 2003. Viscoelastic scaling of colloidal gels in polymer solutions. Langmuir 19 (9), 3589–3595. https://doi.org/10.1021/la026087e.

Paul, F., Morin, A., Monsan, P., 1986. Microbial polysaccharides with actual potential industrial applications. Biotechnol. Adv. 4 (2), 245–259. https://doi.org/10.1016/0734-9750(86)90311-3.

Persello, J., Boisvert, J.P., Guyard, A., et al., 2004. Structure of nanometric silica clusters in polymeric composite materials. J. Phys. Chem. B 108 (28), 9678–9684. https://doi.org/10.1021/jp031249g.

Petit, L., Bouteiller, L., Brulet, A., et al., 2007. Responsive hybrid self-assemblies in aqueous media. Langmuir 23 (1), 147–158. https://doi.org/10.1021/la061466j.

Pi, G., Li, Y., Bao, M., et al., 2016. Novel and environmentally friendly oil spill dispersant based on the synergy of biopolymer xanthan gum and silica nanoparticles. ACS Sustain. Chem. Eng. 4 (6), 3095–3102. https://doi.org/10.1021/acssuschemeng.6b00063.

Pooja, D., Panyaram, S., Kulhari, H., et al., 2014. Xanthan gum stabilized gold nanoparticles: characterization, biocompatibility, stability and cytotoxicity. Carbohydr. Polym. 110, 1–9. https://doi.org/10.1016/j.carbpol.2014.03.041.

Rochefort, W.E., Middleman, S., 1987. Rheology of xanthan gum: salt, temperature, and strain effects in oscillatory and steady shear experiments. J. Rheol. 31 (4), 337–369. https://doi.org/10.1122/1.549953.

Sato, T., Norisuye, T., Fujita, H., 1984. Double-stranded helix of xanthan: dimensional and hydrodynamic properties in 0.1 M aqueous sodium chloride. Macromolecules 17 (12), 2696–2700. https://doi.org/10.1021/ma00142a043.

Senanayake, K.K., Mukhopadhyay, A., 2019. Nanoparticle diffusion within dilute and semidilute xanthan solutions. Langmuir 35 (24), 7978–7984. https://doi.org/10.1021/acs.langmuir.9b01029.

Shchipunov, Y.A., Tyy, Karpenko, Krekoten, A.V., 2005a. Hybrid organic–inorganic nanocomposites fabricated with a novel biocompatible precursor using sol-gel processing. Compos. Interfac. 11 (8–9), 587–607. https://doi.org/10.1163/1568554053148816.

Shchipunov, Y.A., Karpenko, T.Y., Krekoten, A.V., et al., 2005b. Gelling of otherwise nongelable polysaccharides. J. Colloid Interface Sci. 287 (2), 373–378. https://doi.org/10.1016/j.jcis.2005.02.004.

Shoichet, M.S., 2010. Polymer scaffolds for biomaterials applications. Macromolecules 43 (2), 581–591. https://doi.org/10.1021/ma901530r.

Srivastava, S., Schaefer, J.L., Yang, Z., et al., 2014. 25th anniversary article: polymer–particle composites: phase stability and applications in electrochemical energy storage. Adv. Mater. 26 (2), 201–234. https://doi.org/10.1002/adma.201303070.

Tako, M., Teruya, T., Tamaki, Y., et al., 2009. Molecular origin for rheological characteristics of native gellan gum. Colloid Polym. Sci. 287 (12), 1445–1454. https://doi.org/10.1007/s00396-009-2112-2.

Trappe, V., Weitz, D., 2000. Scaling of the viscoelasticity of weakly attractive particles. Phys. Rev. Lett. 85 (2), 449. https://doi.org/10.1103/PhysRevLett.85.449.

Wang, J., Somasundaran, P., 2007. Study of galactomannose interaction with solids using AFM, IR and allied techniques. J. Colloid Interface Sci. 309 (2), 373–383. https://doi.org/10.1016/j.jcis.2006.10.086.

Wang, F., Wang, Y.J., Sun, Z., 2002. Conformational role of xanthan in its interaction with locust bean gum. J. Food Sci. 67 (7), 2609–2614. https://doi.org/10.1111/j.1365-2621.2002.tb08786.x.

Wang, Z.Y., Lin, M.Q., Li, H.K., et al., 2022. Plugging property and displacement characters of a novel high-temperature resistant polymer nanoparticle. Petrol. Sci. 19 (1), 387–396. https://doi.org/10.1016/j.petsci.2021.08.010.

Wyatt, N.B., Gunther, C.M., Liberatore, M.W., 2011. Increasing viscosity in entangled polyelectrolyte solutions by the addition of salt. Polymer 52 (11), 2437–2444. https://doi.org/10.1016/j.polymer.2011.03.053.

Xin, X., Xu, G., Gong, H., et al., 2008. Interaction between sodium oleate and

partially hydrolyzed polyacrylamide: a rheological study. Colloid. Surface. 326 (1–2), 1–9. https://doi.org/10.1016/j.colsurfa.2008.05.009.
Xu, L., Xu, G., Liu, T., et al., 2013. The comparison of rheological properties of aqueous welan gum and xanthan gum solutions. Carbohydr. Polym. 92 (1), 516–522. https://doi.org/10.1016/j.carbpol.2012.09.082.
Xu, L., Xu, G., Yu, L., et al., 2014. The displacement efficiency and rheology of welan gum for enhanced heavy oil recovery. Polym. Adv. Technol. 25 (10), 1122–1129. https://doi.org/10.1002/pat.3364.
Xu, L., Gong, H., Dong, M., et al., 2015. Rheological properties and thickening mechanism of aqueous diutan gum solution: effects of temperature and salts. Carbohydr. Polym. 132, 620–629. https://doi.org/10.1016/j.carbpol.2015.06.083.
Xu, L., Liu, S., Qiu, Z., et al., 2021. Hydrophobic effect further improves the rheological behaviors and oil recovery of polyacrylamide/nanosilica hybrids at high salinity. Chem. Eng. Sci. 232, 116369. https://doi.org/10.1016/j.ces.2020.116369.
Xue, D., Sethi, R., 2012. Viscoelastic gels of guar and xanthan gum mixtures provide long-term stabilization of iron micro-and nanoparticles. J. Nano Res. 14 (11), 1–14. https://doi.org/10.1007/s11051-012-1239-0.
Yi, S., Babadagli, T., Li, H., 2020. Stabilization of nickel nanoparticle suspensions with the aid of polymer and surfactant: static bottle tests and dynamic micromodel flow tests. Petrol. Sci. 17 (4), 1014–1024. https://doi.org/10.1007/s12182-020-00433-1.
Zhang, J., Yang, Z., Zhang, H., et al., 2019. Hydrogels consisting of vesicles constructed via the self-assembly of a supermolecular complex formed from α-cyclodextrin and perfluorononanoic acid. Langmuir 35 (51), 16893–16899. https://doi.org/10.1021/acs.langmuir.9b03140.
Zhou, W., Xin, C., Chen, S., et al., 2020. Polymer-enhanced foam flooding for improving heavy oil recovery in thin reservoirs. Energy Fuel. 34 (4), 4116–4128. https://doi.org/10.1021/acs.energyfuels.9b04298.